Computational Fluid Dynamics Model to Simulate Methane Dispersion at Oktoberfest

Sebastian Lober[1], Florian Dietrich[2], and Jia Chen[1]

[1]Environmental Sensing and Modeling, Technical University of Munich (TUM), Munich, Germany
[2]Environmental Sensing and Modeling

November 24, 2022

Abstract

In this paper, a computational fluid dynamics (CFD) model is developed to simulate the methane (CH4) dispersion of exhaust gases from the Munich Oktoberfest, the world's largest folk festival. Since we assume CH4 losses during the natural gas driven heating and cooking process, our aim is to provide a methodology for estimating these emissions. We developed a forward CFD dispersion model and combined it with on-the-site backpack measurements to quantify the emissions at the festival. The emission number is determined by scaling the simulated to the measured concentrations. Our sensitivity study reveals that the turbulent Schmidt number and the measured wind speed have high impacts on the emission results. Further, we investigated the effect of buoyancy, since there is a temperature gradient between the exhaust gases and the environment. Our results show that the buoyancy is an important factor for assessing hot emissions. Finally, we compared our findings to results determined by a Gaussian plume model and discussed advantages and disadvantages of each approach. Our findings show that CFD models can reproduce real dispersion processes in very complex environments with a high spatial resolution and are able to predict emissions. This study offers a completely new methodology to quantify local emissions on a real scale array and presents one of the first attempts to use CFD to study superimposed greenhouse gas sources.

Computational Fluid Dynamics Model to Simulate Methane Dispersion at Oktoberfest

Sebastian Lober[1], Florian Dietrich[1], and Jia Chen[1]

[1]Environmental Sensing and Modeling, Technical University of Munich (TUM), Munich, Germany

Key Points:

- A computational fluid dynamics (CFD) model to simulate the methane dispersion of Oktoberfest was developed.
- In combination with concentration measurements, the model developed can be used to quantify methane emissions of large area sources.
- The impact of various input parameters, e.g. turbulent Schmidt number, wind and buoyancy on the results are quantified.

Corresponding author: Sebastian Lober, `sebastian.lober@tum.de`

Corresponding author: Jia Chen, `jia.chen@tum.de`

Abstract

In this paper, a computational fluid dynamics (CFD) model is developed to simulate the methane (CH_4) dispersion of exhaust gases from the Munich Oktoberfest, the world's largest folk festival. Since we assume CH_4 losses during the natural gas driven heating and cooking process, our aim is to provide a methodology for estimating these emissions. We developed a forward CFD dispersion model and combined it with on-the-site backpack measurements to quantify the emissions at the festival. The emission number is determined by scaling the simulated to the measured concentrations. Our sensitivity study reveals that the turbulent Schmidt number and the measured wind speed have high impacts on the emission results. Further, we investigated the effect of buoyancy, since there is a temperature gradient between the exhaust gases and the environment. Our results show that the buoyancy is an important factor for assessing hot emissions. Finally, we compared our findings to results determined by a Gaussian plume model and discussed advantages and disadvantages of each approach. Our findings show that CFD models can reproduce real dispersion processes in very complex environments with a high spatial resolution and are able to predict emissions. This study offers a completely new methodology to quantify local emissions on a real scale array and presents one of the first attempts to use CFD to study superimposed greenhouse gas sources.

1 Introduction

Climate warming is affecting the environment all over the world. Events and changes can be observed which did not occur before. Melting of the ice caps, severe floods, droughts, heat waves and the rising sea level (Bailey & Callery, 2020) are just some examples of possible consequences. A NASA and NOAA analysis (NOAA National Centers for Environmental Information, 2020) reveals the last decade as the hottest on record and 2019 the second warmest year on record. One reason for the present global warming period are the strong greenhouse gas (GHG) emissions. The rate of the rising temperature is unprecedented compared to the past 66 million years (Zeebe et al., 2016). The two most dominant GHGs are carbon dioxide (CO_2) and methane (CH_4). While CO_2 is already a well-known and widely researched GHG, CH_4 comes more and more in the scientific focus. CH_4 is about 86-times as effective as the same mass amount of CO_2 over a time period of 20 years and 28-times as powerful on a 100 year time scale with respect to its global warming potential (Jackson et al., 2020). In 2007 the CH_4 concentration began to rise after a 7 year period of stagnation (Mikaloff-Fletcher & Schaefer, 2019; Nisbet et al., 2019). Recent studies (Jackson et al., 2020; Saunois et al., 2020) report for the year 2017 a new record high in CH_4 emissions worldwide. CH_4 is responsible for 23 % of the global warming caused by anthropogenic GHGs (Saunois et al., 2020). More than 600 million tons of the gas were released to the earth's atmosphere and more than halve of it is caused by human activities according to the authors. While wetlands account for roughly one third of the overall emissions, 20 % to 25 % each come from agriculture/waste and fossil fuel sources. Further, Plant et al. (2019) and Varon et al. (2019) recently observed significant CH_4 emissions caused by fossil fuel sources.

In order to react and counteract the global warming process, the origin of the GHG plays a key role. When a reduction of emissions is targeted, mainly emissions caused by fossil fuel burning can be tackled, since they are often directly attributable to human activities and can be replaced by alternative processes and techniques. (Nisbet et al., 2020; Ganesan et al., 2019). In order to improve/avoid CH_4 releasing mechanisms and to reduce the impact on climate warming, a model can be built up based on the data gained from possible sources.

This study investigated the largest folk festival of the world, the Munich Oktoberfest. Here, CH_4 emissions are not only a consequence of the high number of visitors, since other possible reasons for unwanted CH_4 release are pipeline leakages and incomplete combustion of natural gas by kitchen appliances and heat generators as indicated by Chen et al. (2020). During the entire festival period in 2019, 185 000 cubic meters of natural gas were consumed (Landeshauptstadt München, 2019). In order to reconstruct the release of fossil CH_4/natural gas and to quantify possible sources, a model was developed based on CH_4 measurements inside and outside Oktoberfest 2019.

Such models can be based on numerical simulations, relating the exhaust gases of the emission sources and the concentration measurements of the GHGs. For predicting the sources' quantitative impact, Gaussian plume models (Chen et al., 2020) can be used. Their results are often very coarse, since no real geometry of the environment is taken into account and the air flow in the region of interest is not simulated. Another approach to obtain emission origins and their behaviour are computational fluid dynamics (CFD) simulations. Here, for creating an appropriate fluid flow model, the spatial resolution of the flow fields is essential. Mesoscale models, such as the Weather Research and Forecasting (WRF) model (Beck et al., 2012; Zhao et al., 2019), work with a grid resolution of about 1 km. In order to analyze emission processes more in detail and to include typical GHG sources, such as buildings, power plants, factories and vehicles, the micro-scale approach is more suited. A combination of both scale models is presented by Berchet et al. (2017), who used mesoscale patterns to serve as boundary conditions for a microscale urban flow model. The PALM project (Maronga et al., 2020) also offers urban applications of atmospheric boundary-layer flows from meso- to microscale. Since the festival investigated in this paper takes place at a small isolated area of 0.42 km^2 and background measurements are available, we used the mircoscale approach for our simulation model.

To provide an overview of the current state of the art in this field, Lateb et al. (2016); Meroney et al. (2016); Tominaga and Stathopoulos (2013) summarized previous projects and milestones. Tominaga and Stathopoulos (2007, 2016); Gromke and Blocken (2015); Yu and Thé (2017); Shi et al. (2008) developed CFD models for simulating pollutant dispersion in urban areas by validating them with wind tunnel data. Idrissi et al. (2018); Wingstedt et al. (2017); Wang et al. (2015) simulated CH_4 and CH_4 based natural gas dispersion in cities by using this method. Simulations based on real geometry are much rarer. A CH_4 emission estimation of a landfill site close to Ipswich (UK) was done by Sonderfeld et al. (2017) using CFD and in situ measurements. Jeanjean et al. (2015); Nozu and Tamura (2012); Van Hooff and Blocken (2010); Patnaik et al. (2007); Hanna et al. (2006) show CFD model approaches in real cities, which are validated by on-site measurements. The only study, which faces the flow of contaminated exhausts emitted by a chimney (up to the authors' knowledge) was done by Toja-Silva et al. (2017). They simulated the CO_2 dispersion from an urban power plant inside the city of Munich (Germany) and validated their findings with on-site measurements. They also analyzed the spatial distribution of CO_2 concentrations by presenting a concentration map.

However, the emissions of temporary events such as folk festivals have never been modelled numerically using CFD. This study also offers a completely new methodology to quantify local emissions and presents one of the first attempts to use CFD to investigate superimposed GHG sources on a real scale array.

2 Methodology

In this study a CFD simulation is applied to model the CH_4 dispersion based on CH_4 and wind measurements. Using the measurements and the simulation outcomes, the CH_4 emissions were quantified.

2.1 Measurements

As measurement device the LI-COR LI-7810 CH4/CO2/H2O Gas Analyzer was chosen. The gas tracer uses optical feedback-cavity enhanced absorption spectroscopy to analyze the current CH_4 concentration. It captures one sample per second and determines the CH_4 proportion with a precision of 0.25 ppb (5 s averaging) (LI-COR Inc., 2018). Because the instrument has no GPS tracker, a smartphone application was used to record the position of each measurement continuously.

The backpack measurements were split into two different parts: individual surveys inside and outside the festival area. Both are called rounds in the following. For the measurements outside Oktoberfest, the shortest path around the perimeter of the festival premises (Theresienwiese) was chosen. The measurements on Theresienwiese were made following a route, which covered as many potential pollution spots as possible. The route leads through the two main and some side streets (for exact path see Figure C1).

In order to validate measured CH_4 peaks at Oktoberfest, the consideration of wind direction and speed is essential. The exact wind conditions must be also known in order to set up a CFD simulation, since the fluid flow has to be defined explicitly. For these reasons, the wind measurements were taken as close to the festival as possible, which was a location 150 m away from the festival premises. They were recorded on top of a 26 m high building, which is located at 48.134188° N and 11.545524° E. The sensor used is a Lufft WS200-UMB 2D ultrasonic anemometer. Since we implement a whole round in the simulation, the wind conditions recorded at a rate of 1 Hz had to be averaged over the time required to complete a round around the perimeter of Oktoberfest.

The round, which was investigated in this study, was selected on the basis of the following parameters. The standard deviation of the wind direction and speed should be low, the measured concentration peaks should be clearly visible and the wind direction should roughly match the concentration distribution. Further, the measured wind speed of the round should not be below $1.5\,\mathrm{m\,s^{-1}}$ at dispersion height (which leads to a minimum of $2\,\mathrm{m\,s^{-1}}$ at wind measurement height). The round, which fitted best to the criteria, was recorded on September 29 at 4:45 pm (UTC). The wind characteristics of this round (mean value ± standard deviation) are $(240.5 \pm 12.9)°$ and $(2.75 \pm 0.91)\,\mathrm{m\,s^{-1}}$.

2.2 Governing Equations of the Fluid Flow

The simulation progress is divided into two steps. First, the wind flow is simulated by the steady-state Reynolds-Averaged Navier-Stokes (RANS) equations, together with a modified standard k-ϵ model (Durbin, 1996). Based on the solved wind field, the CH_4 dispersion is obtained by applying the unsteady convection-diffusion equation. During the wind flow calculation step the exhaust is treated like air, while for the passive-scalar gas transport calculation the exhaust emissions contain a specific amount of CH_4. The model was executed as incompressible first and for the sensitivity study, we also investigated the compressible case. All numerical calculations are carried out using the open-source software environment OpenFOAM.

2.2.1 Fluid Flow Equations

This study applies the concept of Reynolds. With the RANS equations, larger scale systems can be modelled and the computational cost is the lowest compared to Direct Numerical Simulations (DNS) and Large Eddy Simulations (LES). Besides that, LES simulations produce not necessarily better results compared to RANS models, due to high uncertainties of atmospheric models in real urban environments (Patnaik et al., 2007). Therefore, the use of RANS is usually most efficient, when highly accurate results of very turbulent flows are not required (Tominaga & Stathopoulos, 2016). The following section gives a short overview on the theory used in the simulation.

On the basis of the well-known Navier-Stokes equations, the expressions for the RANS were developed. They consist of the momentum equation and the mass conservation (here in an incompressible form with constant viscosity and density).

$$\rho\frac{\partial \overline{u}_i}{\partial t} + \rho\frac{\partial}{\partial x_j}(\overline{u}_i\overline{u}_j) = -\frac{\partial \overline{p}}{\partial x_i} + \mu\left(\frac{\partial \overline{u}_i}{\partial x_j} + \frac{\partial \overline{u}_j}{\partial x_i}\right) - \rho\frac{\partial}{\partial x_j}(\overline{u_i'u_j'}) \tag{1}$$

$$\frac{\partial \overline{u}_i}{\partial x_i} = 0 \tag{2}$$

where u represents the velocity, p is the air pressure, ρ stands for the air density and μ is dynamic viscosity.

For this project, the turbulence model applied is based on the standard k-ϵ model. The approach assumes that the flow is fully turbulent and consequently the effects of molecular viscosity are negligible. On the basis of the standard k-ϵ model, some modifications were made to increase the accuracy. Kato and Launder (1993); Tsuchiya et al. (1997); Yap (1987) made suggestions for improvements, especially tackling the overestimation of the turbulent kinetic energy in the impinging region of bluff bodies. Another approach is the modification of ν_t which is used in our model. Durbin (1996) proposed the calculation of ν_t by coupling it to the turbulence time scale T. This approach was developed specifically for simulations with wind flow in urban environments and verified for exhaust dispersion applications by investigating a benchmark case (Toja-Silva et al., 2015). This turbulence model is applied in the following. The values of the coefficients used in the turbulence equations are based on physical experiments. Here the standard values ($C_\mu = 0.09, \quad C_{\epsilon 1} = 1.44, \quad C_{\epsilon 2} = 1.92, \quad \sigma_k = 1.0, \quad \sigma_\epsilon = 1.3$) suggested by Pope (2000) are used.

2.2.2 Gas Dispersion Equations

The convection-diffusion passive scalar equation for incompressible turbulent flows gives a possible solution for the gas concentration fields. The equation consists of a transient, a convection and a diffusion term.

$$\frac{\partial C}{\partial t} + \frac{\partial \overline{u}_j C}{\partial x_j} - \frac{\partial}{\partial x_j}\left(D_{eff}\frac{\partial C}{\partial x_j}\right) = 0 \tag{3}$$

Here, the volumetric averaged gas concentration is represented by C. $D_{eff} = D + D_t$ is the effective diffusivity. The molecular diffusivity D depends on the kind of gas and the medium surrounding it, and can be found in appropriate literature (Lide, 2004). The eddy diffusivity D_t can be determined by

$$D_t = \frac{\nu_t}{Sc_t} \tag{4}$$

where Sc_t is the turbulent Schmidt number and ν_t represents turbulent viscosity. For pollutant dispersion in environmental flows, Tominaga and Stathopoulos (2007); Blocken et al. (2007); Gualtieri et al. (2017) suggest an acceptable range of 0.1 to 1.0 for Sc_t. Since Sc_t depends on the characteristics of the flow and the location in the flow pattern, it is important where the region of interest is. For plume dispersion downwind and its longitudinal transport, small values of Sc_t are suggested by previous studies (Tran et al., 2019; Yu & Thé, 2017). These circumstances are given in this study, which is why a small Sc_t is beneficial. Furthermore, trace gas concentrations close to the ground and buildings are better predicted, when a low turbulent Schmidt number compensates a high turbulent diffusion of momentum, which is often underestimated at these locations (Riddle et al., 2004; Di Sabatino et al., 2007; Blocken et al., 2008; Nakibolu et al., 2009). Especially in our case, a high turbulent kinetic energy can be found due to many complex obstacles which exist on a public festival. Therefore, this study applies a comparatively low Schmidt number of 0.4 as suggested by Yu and Thé (2017), but also investigates the impact of using different values in the sensitivity study.

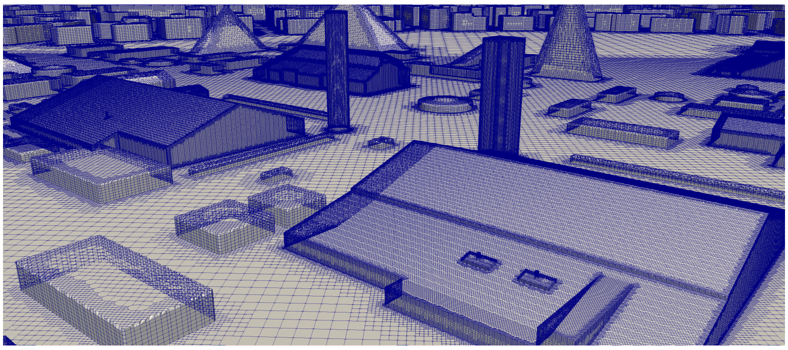

Figure 1. Numerical simulation geometry as a 16 million cell mesh.

2.3 Numerical Domain and Grid Generation

The geometry model used in this simulation is designed with the CAD tool AutoCAD. Large beer tents (>1000 seats) and buildings on and next to the festival area were constructed in the model. However, since the Oktoberfest geometry is very complex, not everything was covered precisely by the model. Humans, small booths and various fairground rides are hard to model with the given information and a static geometry. Therefore, a simplified geometry was included for these installations at Oktoberfest. The dimensions of the geometries were gathered using satellite images provided by Google, Maxar Technologies.

The dimensions of the Cartesian simulation domain are created in OpenFOAM on the basis of the CFD simulation best practice guidelines (Franke et al., 2007). The final model, which includes tents and buildings, has about 16 million cells and is shown in Figure 1.

2.4 Boundary Conditions

Since RANS equations are used in the CFD model, we applied a velocity-inlet and pressure-outlet for the simulation domain. The remaining boundaries are defined by fixed values, zero gradients and standard wall functions (for an overview of all conditions see Table A1, A2).

At the inlet boundary, where the wind flows into the domain, the measured wind and turbulence conditions are imposed to the model. In order to apply the measured wind speed to the inlet, the equations of Richards and Hoxey (1993) are used. With this approach, the vertical velocity profile, the kinetic energy and the dissipation rate profile of the inlet can be determined. A fixed value is applied for the pressure at the outlet which represents the outflow boundary in the domain.

At the chimney boundaries, a fixed exhaust velocity u_{exh} is applied. It is estimated by the flue-gas stack draft. The relations are derived from Klote (1991). For estimating the flue-gas flow-rate, the molar mass of the exhaust and the surrounding air are assumed to be equal and the frictional resistance and heat losses are negligible.

$$u_{exh} = C\sqrt{2gh\frac{T_i - T_o}{T_i}} \tag{5}$$

The gravity acceleration g is chosen as $9.81\,\mathrm{m\,s^{-2}}$ and h represents the height of the chimney. For the discharge coefficient C, a value of 0.6 is usually assumed. With a chimney height of 6 m and an approximated temperature difference of 80 °C, an exhaust velocity u_{chim} of approximately $3\,\mathrm{m\,s^{-1}}$ is determined. The exhaust temperature is based on

Sadeghzadeh (2007); Dudkiewicz and Szaaski (2020) and selected by considering the circumstances in the kitchens, such as heat losses between the devices and the chimney system. Since not every tent has the same guest capacity and thus various amounts of cooking and heating is done, the different number of available seats have to be taken into account. Therefore, the amount of emitted exhausts were modified for every single tent. We assumed that all natural gas fueled devices have the same CH_4 leakage rate and therefore all exhaust flows should have the same CH_4 concentration. If a tent has a higher capacity, more grills and heat generators are suspected. Hence, the outlet flow rises, since the geometry of all chimneys is assumed identical. The average of all outlet velocities is $3\,\mathrm{m\,s^{-1}}$. For the calculation, all seats inside and outside the tents are considered.

For the ground boundary, the sand-grain based fully rough law (Blocken et al., 2007) is used to impose roughness to the boundary surface. The aerodynamic roughness length z_0 is defined to be 0.2 m and for the roughness constant C_s a value of 7 is recommended by Van Hooff and Blocken (2010). This results in a roughness height $k_s = 0.2798$ m according to equation 6.

$$k_s = \frac{9.793 \cdot z_0}{C_s} \tag{6}$$

The roughness height of the the tents and buildings is set to zero ($k_s = 0$).

In the second part of the simulation, which simulates the transport and diffusion of CH_4, the velocity field and the turbulent viscosity are given through the fluid flow simulation and are used as fixed boundary conditions. The background and exhaust concentrations are applied at the boundaries. The determination of the background for the selected round is done by calculating the mean of all concentration values below the 10 % quantile. The exhaust concentration of the chimneys is varied to scale the resulting simulation concentrations to the measurements (see section 2.6).

2.5 Numerical Procedure and Implementation

The fluid flow simulation of the main model was performed by the incompressible OpenFOAM solver *simpleFOAM* for turbulent flows, which uses the SIMPLE (Semi-Implicit Method for Pressure Linked Equations) algorithm to solve the RANS equations. The fluid flow part of the simulation uses Gaussian second order linear interpolation schemes. The residuals for the fluid flow are below 1×10^{-5}.

The diffusion problem is solved by a customized solver $turbulentScalarTransportFoam$, which was previously created by Toja-Silva et al. (2017). It extends the $scalarTransportFoam$ solver by including the turbulent eddy dissipation.

The calculations are carried out on the Linux Cluster of the Leibniz Supercomputing Centre (LRZ) on 64 cores in parallel.

2.6 Determining the Emission Number

In order to determine a total emission number of Oktoberfest, we used the approach as described in Chen et al. (2020) to scale the prior emission number of the forward CFD simulation until the modelled and measured curve match (see Figure 4). For that purpose, the chimneys' exhaust concentration C_{exh,CH_4} is varied until the areas underneath the measurement and simulation plume curves are equal. Only the measurements outside the Oktoberfest premises were used, as the measurements inside are too much distorted by local emission sources, such as humans and small booths that we neglected in the model. We considered only the chimneys of the large tents (>1000 seats) as CH_4 emitters. These chimneys are modelled with an exhaust outflow concentration C_{exh,CH_4}. The mean exhaust velocity of all chimneys u_{exh} is $3\,\mathrm{m\,s^{-1}}$ and the radius of a single chimney r_{chim} is 0.3 m. All $n_{chims} = 17$ chimneys have an identical geometry. That information together with the area of Oktoberfest can be used to calculate the overall emission number:

$$E = \frac{\rho_{air} \cdot M_{CH_4} \cdot C_{exh,CH_4} \cdot A_{chim} \cdot u_{exh} \cdot n_{chims}}{M_{air} \cdot A_{Oktoberfest}} \tag{7}$$

where $\rho_{air} = 1204\,\mathrm{g\,m^{-3}}$ is the density of air at 20 °C and $M_{air} = 28.94\,\mathrm{g\,mol^{-1}}$ represents the molar mass of dry air. $M_{CH_4} = 16.04\,\mathrm{g\,mol^{-1}}$ refers to the molar mass of CH_4, while $A_{chim} = 0.28\,\mathrm{m^2}$ is the cross section area of a single chimney. The part of Theresienwiese, where Oktoberfest takes place, is about $A_{Oktoberfest} = 420\,000\,\mathrm{m^2}$.

2.7 Sensitivity Study

The simulation model is based on some input parameters, for which no uniform values are suggested in the literature or are not known precisely. For these parameters, a sensitivity analysis was performed to figure out how much variations in these input parameters affect the output.

The choice of the turbulent Schmidt number Sc_t depends on the kind of study and can vary between 0.1 and 1.0 (Tominaga & Stathopoulos, 2007; Blocken et al., 2007; Gualtieri et al., 2017). Based on Yu and Thé (2017), we decided to use 0.4 in this study. However, we ran the simulation also for the numbers 0.2, 0.6 and 0.8 to quantify the uncertainty of choosing a different Schmidt number.

The wind speed and direction fluctuates during a walked measurement round, which took about 35 min. Therefore, the simulations were carried out once using the mean values of the wind speed and direction and two additional times using the wind parameters obtained by subtracting and adding the standard deviation during the measurement round.

The averaged value of the chimneys' exhaust velocities $3\,\mathrm{m\,s^{-1}}$ is estimated on the basis of the exhaust temperatures of the kitchen appliances used (see equation 5). In order to account for the large possible variations in exhaust temperatures, we ran the simulations also for exhaust velocities of $2\,\mathrm{m\,s^{-1}}$ and $4\,\mathrm{m\,s^{-1}}$.

Since the exhaust gas, which is emitted by the chimneys, has a specific temperature, which is significantly higher than the surrounding air, a model considering the buoyancy effect is developed, too. This simulation consists of a compressible domain, which takes density differences caused by the exhaust temperature into account. When the buoyancy force is included in the simulation, some modified equations are needed. Usually, two approaches are available for including buoyancy effects to the fluid flow: an incompressible model with the Boussinesq approximation or a completely compressible model. The Boussinesq approximation could not be implemented, because the simulation is not fulfilling its usage criterion $\beta(T - T_0) << 1$. Therefore, the model was simulated as compressible. The pressure term in the momentum conservation equation is replaced by a new parameter p'. Here, p' considers hydrostatic pressure effects.

$$p' = p - \rho g z \tag{8}$$

where g is the gravitational acceleration and z the height above the ground. Besides this modification, the energy conservation equation is added, in order to take the exhaust's temperature and therefore the density difference into account. The energy equation is defined as follows:

$$\frac{\partial(\rho h)}{\partial t} + \nabla(\rho u h) + \frac{\partial(\rho K)}{\partial t} + \nabla(\rho u K) - \frac{\partial p}{\partial t} = \nabla(\alpha_{eff} \nabla h) + \rho u g \tag{9}$$

Here, h stands for the enthalpy and K represents the kinetic energy. The effective thermal diffusivity α_{eff} is the sum of laminar and turbulent thermal diffusivities. The temperature used for calculating the exhaust velocity is also used for the chimneys' temperature boundary, when the simulation is run compressible. The OpenFOAM solver *bouynatSimpleFoam* is applied for the compressible model.

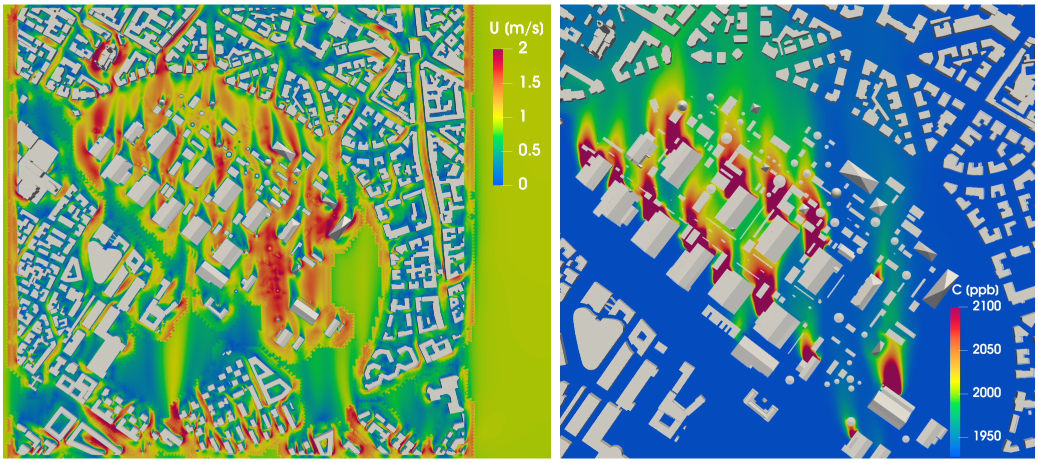

Figure 2. Vertical slice of the flow velocity (left) and the CH_4 concentration (right) at $z = 3\,\mathrm{m}$. The chimney outlets are located at $z = 9\,\mathrm{m}$.

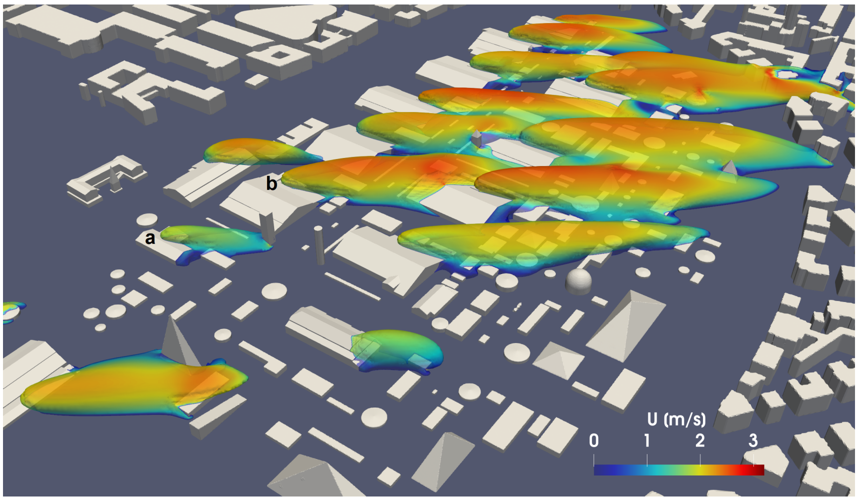

Figure 3. Isosurface corresponding to $C = 1980\,\mathrm{ppb}$. Tent "a"/"b" are marked exemplary for a low/high exhaust velocity u_{exh}.

3 Simulation Results

This section presents the simulation results and the conclusions of the sensitivity study. Subsequently, a comparison to the Gaussian plume model is shown.

3.1 Concentration Distribution and Emission Number

The vertical wind speed and CH_4 concentration distribution in the domain at 3 m height can be seen in Figure 2. There, it is shown that the CH_4 dispersion follows the flow and the concentrations reach the ground right behind the tents. This can be also seen in Figure 3 (for close-up view see Figure B1). The figure shows the plume dispersion in three dimensions and demonstrates that tents with a lower CH_4 outflow velocity, such as chimney "a", produce smaller plumes than those with a higher one, such as chimney "b". The concentration distribution on the round around the premises is shown in Figure 4. Here, the unit of the x-axis represents the position on the track around the

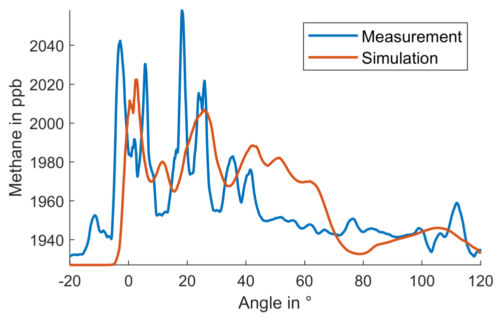

Figure 4. Measurement and scaled simulation concentration trend on the outside part of the round. The angle defines the position on the outside track (0°=N; 90°=E).

perimeter of Oktoberfest. 0° stands for the point on the round, which intersects a north-pointing line from the premises-center. Analogously, 90° is the eastern crossing point on the round. The figure presents the concentration plume curves on the track on ground level of the measurements and the simulation. It can be seen that the plume simulated by the CFD model (brown curve) match the measurements (blue curve) regarding the position on the track and resemble the shape of the measurement plume curve well. Overall, there is a strong correlation between the CFD model result and the outside measurements as R^2 reaches a values of 0.55 (R=0.74). The resulting emission number is $5.33\,\mu g\,m^{-2}\,s^{-1}$.

While the result of the outside round is used to determine the emission number, also concentrations inside the festival area were compared to the measurements. In contrast to the measurements outside the festival area, the result for inside shows less correlation as R^2=0.05 (R=0.22) between the measured and modelled concentrations. Those findings suggest that inside the Oktoberfest area the influence of the chimneys' exhaust is superimposed by small local sources that were not modelled in this study, such as open tent doors and windows, gas heaters in the beer gardens, gas grills in the streets etc. Furthermore, not all obstacles such as fair rides, small booths and humans are included in the model, which is the reason why the model performs worse for the near field.

3.2 Sensitivity Study

The input parameters, which can not be precisely determined by relevant literature or measurements, were varied, in order to analyze their impact on the result. Table 1 summarizes the parameters, which are used for the uncertainty assessment and shows their impact on the emission number.

3.2.1 Turbulent Schmidt number

Besides the chosen value of of 0.4 for the turbulent Schmidt number, the resulting plume curves for the values 0.2, 0.6 and 0.8 can be seen in Figure 5 (top-left). It is visible that the absolute concentration values are highly dependent on the choice of the turbulent Schmidt number. A higher Sc_t leads also to higher concentrations on ground level. This means that increasing the value will reduce therefore the emission number and vice versa. The emission number is therefore significantly dependent on the turbulent Schmidt number.

As pointed out in section 2.2.2, the Schmidt number depends on the observing position in the flow. For locations downwind, where CH_4 is transported longitudinal, low numbers are suggested (Tran et al., 2019; Yu & Thé, 2017). Further, close to the ground

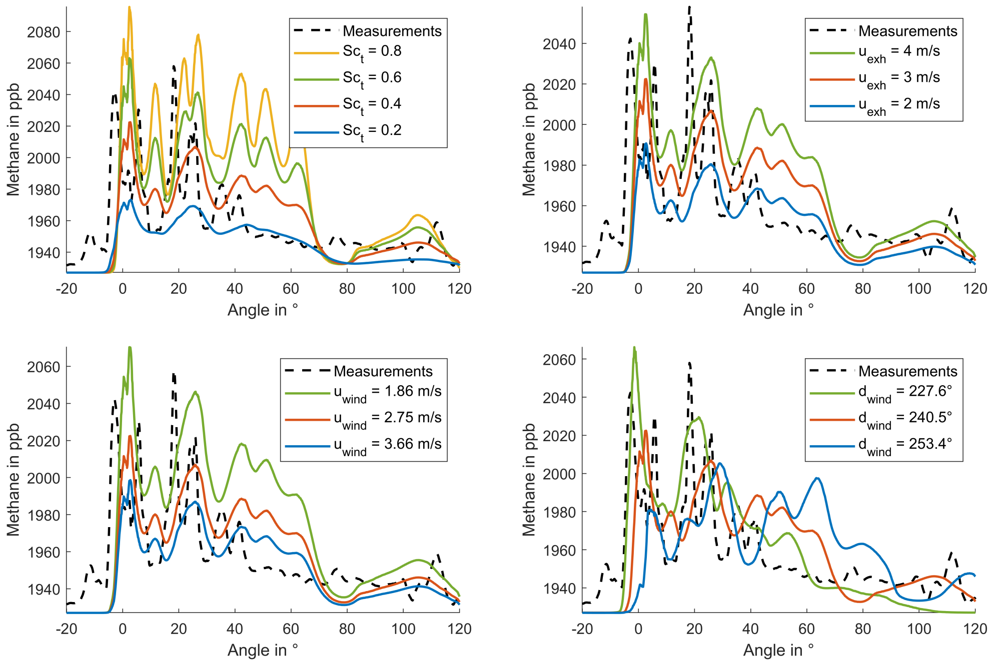

Figure 5. CH_4 concentration distribution for different turbulent Schmidt numbers (up-left), different mean chimney exhaust velocities (up-right), the measured wind speed (bottom-left) and wind direction (bottom-right) with its standard deviation. All cases use an exhaust concentration of C_{exh} = 191 ppm (0°=N; 90°=E).

and buildings, a small Sc_t compensates the turbulent diffusion of momentum, which is often underestimated at these locations (Riddle et al., 2004; Di Sabatino et al., 2007; Blocken et al., 2008; Nakibolu et al., 2009). Since this is given in our case, a Schmidt number lower than standard values around 0.7 is reasonable. On the other hand, decreasing Sc_t affects the spatial dispersion of the trace gas (see Figure 5, top-left). The distribution is more uniform and local peaks get damped. In this study, the selection of 0.4 is a good compromise between capturing the spatial distribution and properly approximating the turbulent kinetic energy at the ground.

3.2.2 Wind Speed and Direction

The wind speed and direction measurements have a mean value and a standard deviation of $(2.75 \pm 0.91)\,\mathrm{m\,s^{-1}}$ and $(240.5 \pm 12.9)°$. The impact of the wind fluctuations, when the standard deviations are applied each, can be seen in Figure 5 (bottom). Generally, the effect of changing wind direction on the simulation results is very dependent on the geometry and level of direction fluctuations. For this investigation, the main part of the plume is slightly shifted. However, the overall concentration level stays similar and thus also the area underneath the plume curve. Therefore, the wind direction has only a limited impact on the emission prediction process (up to 4 %) in this case.

When the wind speed rises, the resulting CH_4 concentration at ground level decreases and as a result the emission number increases proportionally. The wind speed and emission number are therefore positively linearly correlated. Besides the turbulent Schmidt number, the wind speed is essential for assessing source emissions and should be measured carefully.

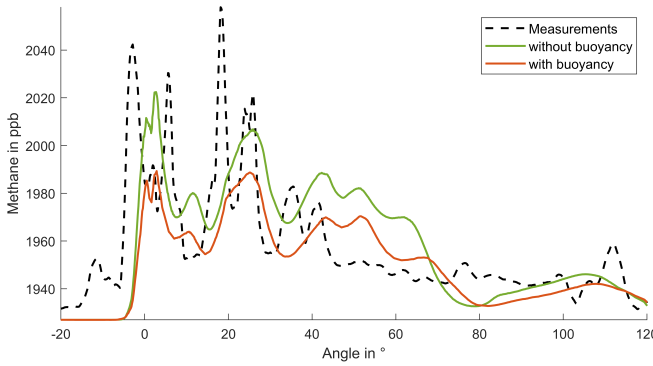

Figure 6. CH_4 concentration distribution with (compressible) and without (incompressible) the buoyancy effect with C_{exh} = 191 ppm (0°=N; 90°=E).

Table 1. Uncertainties and their effect on the emission number (EN).

Type	Value	Deviation	Effect on EN
Turb. Schmidt number	0.4	+/− 0.2	−27 %/+77 %
Wind speed	$2.75\,\mathrm{m\,s^{-1}}$	+/− $0.91\,\mathrm{m\,s^{-1}}$	+33 %/−33 %
Wind direction	240.5°	+/− 12.9°	+2 %/−4 %
Chimney exhaust velocity	$3\,\mathrm{m\,s^{-1}}$	+/− $1\,\mathrm{m\,s^{-1}}$	−0.6 %/+1.1 %

3.2.3 Exhaust Velocity

Figure 5 (top-right) shows the concentration distribution with a u_{exh} of $2\,\mathrm{m\,s^{-1}}$, $3\,\mathrm{m\,s^{-1}}$ (default) and $4\,\mathrm{m\,s^{-1}}$. The qualitative CH_4 dispersion shape for the three variation cases does not change. However, it is clearly visible that the averaged exhaust velocity has a quantitative impact on the resulting CH_4 concentration magnitude. The higher u_{exh} is, the higher the simulated concentrations at ground level. As a result the exhaust CH_4 concentration of the chimneys has to decrease for the simulated ground concentrations to match the measured ones. However, the effect on the emission number is limited, since the emission number is calculated by equation 7, where the lower exhaust concentrations are compensated by the increase of u_{exh}. Therefore, the impact on the predicted number stays at about 1 %. This means that for emission predicting purposes, u_{exh} does not play a key role. However, if the absolute concentration magnitude is the result of interest, the exhaust velocity has a significant impact.

3.2.4 Compressible Approach

In order to understand if and how the emission number is changed by taking the temperature differences between exhaust and the surrounding air into account, we computed the case again, considering buoyancy. For the compressible approach, an air density gradient is allowed in the domain. Figure 6 shows that this approach has a significant impact on the results. Considering buoyancy, the gas stream is lifted upwards, which results in a lower concentration at the ground. Therefore, the emission number rises due to the higher chimney exhaust concentration, which is needed to compensate that effect. Numerically, the effect causes an increase of the emission number from 5.33 to $7.24\,\mathrm{\mu g\,m^{-2}\,s^{-1}}$ (+36 %).

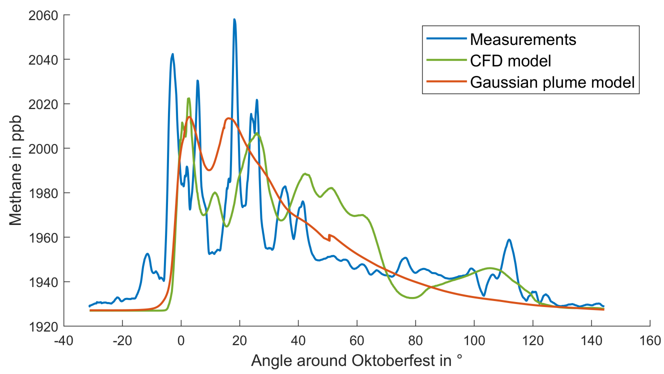

Figure 7. Comparison of scaled results by CFD and Gaussian plume (GP) models for the outside round (0°=N; 90°=E).

3.3 Comparison to Gaussian Plume Model

While the CFD simulation of the exhaust flow of Oktoberfest was done for the first time in this study, a Gaussian plume model was already developed for the Oktoberfest investigation in 2018 (Chen et al., 2020). The Gaussian plume model is a steady-state approach, which simulates the transport of gas emissions and the diffusion released by a point source. The dispersion is represented by a plume which fits the concentration distributions to Gaussian curves in vertical and horizontal directions (Pasquill, 1966, 1969, 1979; Gifford, 1976; Briggs, 1973; Hanna et al., 1982). The results of the two different modeling approaches are compared. In 2018, an average emission number of $(6.7 \pm 0.6)\,\mu g\,m^{-2}\,s^{-1}$ was determined. The emission number found by the present study using CFD and considering buoyancy, is $7.24\,\mu g\,m^{-2}\,s^{-1}$, which is within the uncertainty range of the number determined in 2018 using the Gaussian plume model. We conclude that both Gaussian plume and CFD simulations are suitable for emission estimates of area sources using the approach presented in Chen et al. (2020).

Figure 7 shows scaled simulated plume curves on the basis of a CFD simulation and the Gaussian plume model, which was applied using the setup of Chen et al. (2020). Figure 7 shows that there exists a difference in the shape of the two plumes. While the CFD simulation captures more details, such as single peaks, the Gaussian Plume model represents a low-pass filtered version of the signal. We conclude that for investigations, where a high spatial resolutions is needed, the CFD model offers the possibility to reproduce local enhancements in a greater detail. Such a feature is especially helpful to predict concentrations at a certain point or to inversely model emissions using stationary sensors. Gaussian plume models, by contrast, can provide the overall distribution well, which is sufficient to determine the emission number based on mobile measurements. Furthermore, the calculation effort for the Gaussian plume model is significantly less.

4 Conclusion

This article presents a CFD model, simulating CH_4 dispersions in a complex urban environment. For the first time, a large folk festival, in this case the Munich Oktoberfest, was investigated using fluid dynamics simulations with a spatial resolution of 2 m in the regions of interest.

Based on the results of Chen et al. (2020), the big tents are assumed to be the largest CH_4 emitters. For this reason, a CFD model of Oktoberfest was set up, defining the chimneys of each tent as CH_4 sources. Using a RANS model, the dispersion of the gas is simulated. In order to validate the simulation results and determine the emissions, CH_4 concentration measurements with a mobile CH_4 backpack analyzer around and inside Oktoberfest were carried out, too.

The modelled CH_4 concentrations were scaled to the measurements outside Oktoberfest by varying a prior emission number. The result shows that the simulation case match the overall CH_4 distribution shape of the outside measurement round well. Especially, the qualitative allocation of the CH_4 peaks is similar to the distribution of the measurement maxima. However, the modelled concentration distribution inside the festival area looks different compared to the measured values. We suspect local turbulence and additional CH_4 sources (e.g. humans, food stands), which are not considered in the model, to be the reasons. In our case, the CFD model reconstructed downwind concentrations well (R=0.74), but for near-field applications the result was inadequate (R=0.22).

The resulting emission number of the incompressible case is $5.33\,\mu\mathrm{g\,m^{-2}\,s^{-1}}$. When the buoyancy force is considered in the model, the CFD emission number increases, since the CH_4 plume is lifted upwards resulting in lower concentrations at ground level. In this case the emission number rises to $7.24\,\mu\mathrm{g\,m^{-2}\,s^{-1}}$ (+36 %). This number is in the same magnitude as the value found by Chen et al. (2020) using a Gaussian plume model ($6.7 \pm 0.6\,\mu\mathrm{g\,m^{-2}\,s^{-1}}$).

In order to determine how certain the calculated emission number is, we performed a sensitivity study on all decisive input parameters of the model, such as turbulent Schmidt number, wind speed and direction and the exhaust velocity. The turbulent Schmidt number Sc_t has a significant impact on the emissions and simulated concentration distributions. There exists a negative correlation between Sc_t and the emission number, since an increasing Schmidt number leads to a higher longitudinal plume spread. In this study, a value of 0.4 was used for Sc_t. A 50 % higher Schmidt number, leads to a emission number decrease of 27 %. The wind speed is linearly correlated to the emission number. Changing the wind speed by its standard deviation leads to a ±33 % emission number change. The chimneys' exhaust velocity has only an influence on the absolute concentration magnitude, not on the resulting emission number, as an exhaust velocity variation cancels out with the resulting exhaust concentration change when calculating the emissions.

This study shows, how CH_4 concentrations of a complex urban domain, such as Oktoberfest, can be successfully modelled using a spatially highly resolved CFD model. In future studies, it could be beneficial to take more gas sources into account, since the tents' chimneys are not the only emitters of CH_4 as identified by our on-site investigations. Only then, it will be possible to model the near field, i.e. concentrations inside of the premises, accurately. This can be done by extending the geometry and adding surface sources. In addition, LES modelling can be used for simulating dispersed gas of multiple chimney sources in order to compare LES with RANS models regarding the applicability in such complex real urban environments.

Conclusively, this study shows that CFD is a powerful tool for simulating high-resolution atmospheric GHG dispersion caused by multiple trace gas sources in a complex urban domain. In combination with concentration measurements, it can be used to quantify local emissions and estimate the overall impact of these sources to the environment. The advantages of CFD simulation compared to the Gaussian plume model are the very high spatial resolution which can be used to forecast concentrations at specific locations and the possibility to predict emissions using just a few stationary sensor sites.

Table A1. Fluid flow boundary conditions imposed at each boundary of the domain (incompressible model). Nomenclature: Cc = Calculated, fV = fixedValue, iV = inlet value, sl = slip, wF = wall function, zG = zeroGradient.

	U	**k**	ϵ	ν_t	**p**
Inlet	iV	iV	iV	Cc	zG
Outlet	zG	zG	zG	Cc	fV zero
Ground	fV zero	kqR wF	epsilon wF	nutk rough wF	zG
Buildings	fV zero	kqR wF	epsilon wF	nutk wF	zG
Chimneys	iV	iV	iV	Cc	zG
Sky	sl	sl	sl	Cc	sl
Sides	sl	sl	sl	sl	sl

Table A2. Dispersion boundary conditions imposed at each boundary of the domain. Nomenclature: Cc = Calculated, fV = fixedValue, iV = inlet value, sl = slip, zG = zeroGradient.

	u	ν_t	**C**
Inlet	fV	Cc	iV
Outlet	fV	Cc	zG
Ground	fV	fV	zG
Buildings	fV	fV	zG
Chimneys	fV	Cc	iV
Sky	fV	Cc	zG
Sides	fV	sl	zG

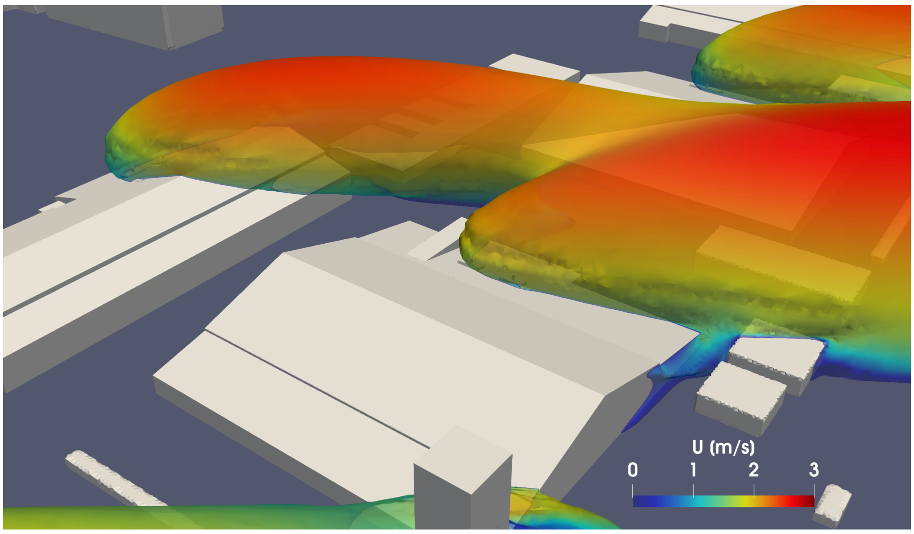

Figure B1. Closer look to the "Schützen" and the "Paulaner" tent.

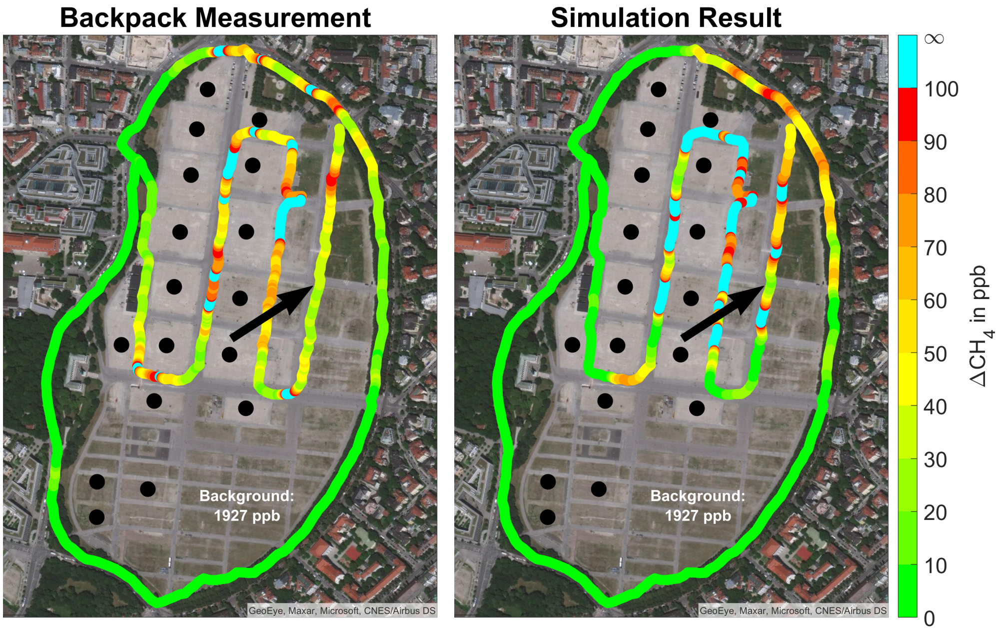

Figure C1. Spatial distribution of measured and simulated CH_4 concentrations outside and inside the Oktoberfest premises with wind direction (arrow) and chimney positions (points). Map provided by Google, Maxar Technologies.

Appendix A Boundary Conditions

Appendix B Close-up View on Chimneys

Appendix C Heatmaps of the measured and simulated CH_4 Concentrations

Acronyms

CFD Computational Fluid Dynamics
DNS Direct Numerical Simulation
GHG Greenhouse Gas
LES Large Eddy Simulation
RANS Reynolds-Averaged Navier-Stokes
SIMPLE Semi-implicit Method for Pressure Linked Equations

References

Bailey, D., & Callery, S. (2020). *The effects of climate change.* `https://climate.nasa.gov/effects/`. (Online; accessed 21-January-2020)

Beck, V., Koch, T., & Kretschmer, R. (2012). Wrf greenhouse gas model (wrf-ghg). *Technical Report*. doi: http://dx.doi.org/10.4126/98-004421262

Berchet, A., Zink, K., Muller, C., Oettl, D., Brunner, J., Emmenegger, L., & Brunner, D. (2017). A cost-effective method for simulating city-wide air flow and pollutant dispersion at building resolving scale. *Atmospheric Environment*, *158*, 181 - 196. doi: https://doi.org/10.1016/j.atmosenv.2017.03.030

Blocken, B., Stathopoulos, T., & Carmeliet, J. (2007). Cfd simulation of the atmospheric boundary layer: wall function problems. *Atmospheric Environment*, *41*(2), 238 - 252. doi: https://doi.org/10.1016/j.atmosenv.2006.08.019

Blocken, B., Stathopoulos, T., Saathoff, P., & Wang, X. (2008). Numerical evaluation of pollutant dispersion in the built environment: Comparisons between models and experiments. *Journal of Wind Engineering and Industrial Aerodynamics*, *96*(10), 1817 - 1831. (4th International Symposium on Computational Wind Engineering (CWE2006)) doi: https://doi.org/10.1016/j.jweia.2008.02.049

Briggs, G. A. (1973). Diffusion estimation for small emissions. preliminary report. doi: https://doi.org/10.2172/5118833

Chen, J., Dietrich, F., Maazallahi, H., Forstmaier, A., Winkler, D., Hofmann, M. E. G., ... Röckmann, T. (2020). Methane emissions from the munich oktoberfest. *Atmospheric Chemistry and Physics*, *20*(6), 3683–3696. Retrieved from `https://acp.copernicus.org/articles/20/3683/2020/` doi: 10.5194/acp-20-3683-2020

Di Sabatino, S., Buccolieri, R., Pulvirenti, B., & Britter, R. (2007). Simulations of pollutant dispersion within idealised urban-type geometries with cfd and integral models. *Atmospheric Environment*, *41*(37), 8316 - 8329. Retrieved from `http://www.sciencedirect.com/science/article/pii/S1352231007005791` doi: https://doi.org/10.1016/j.atmosenv.2007.06.052

Dudkiewicz, E., & Szaaski, P. (2020). Overview of exhaust gas heat recovery technologies for radiant heating systems in large halls. *Thermal Science and Engineering Progress*, *18*, 100522. Retrieved from `http://www.sciencedirect.com/science/article/pii/S2451904920300433` doi: https://doi.org/10.1016/j.tsep.2020.100522

Durbin, P. (1996). On the k-ϵ stagnation point anomaly. *International Journal of Heat and Fluid Flow*, *17*(1), 89 - 90. doi: https://doi.org/10.1016/0142-727X(95)00073-Y

Franke, J., Hellsten, A., Schlnzen, H., & Carissimo, B. (2007). Best practice guideline for the cfd simulation of flows in the urban environment. *COST action*, *732*, 51.

Ganesan, A. L., Schwietzke, S., Poulter, B., Arnold, T., Lan, X., Rigby, M., ... Manning, M. R. (2019). Advancing scientific understanding of the global methane budget in support of the paris agreement. *Global Biogeochemical Cycles*, *33*(12), 1475-1512. Retrieved from `https://agupubs.onlinelibrary.wiley.com/doi/abs/10.1029/2018GB006065` doi: https://doi.org/10.1029/2018GB006065

Gifford, F. A. (1976). Turbulent diffusion-typing schemes: a review. *Nucl. Saf.*, *17*(1), 68-86.

Gromke, C., & Blocken, B. (2015). Influence of avenue-trees on air quality at the urban neighborhood scale. part i: Quality assurance studies and turbulent schmidt number analysis for rans cfd simulations. *Environmental Pollution*, *196*, 214 - 223. doi: https://doi.org/10.1016/j.envpol.2014.10.016

Gualtieri, C., Angeloudis, A., Bombardelli, F., Jha, S., & Stoesser, T. (2017). On the values for the turbulent schmidt number in environmental flows. *Fluids*, *2*, 1-27. doi: 10.3390/fluids2020017

Hanna, S., Briggs, G. A., & Hosker, R. P., Jr. (1982). Handbook on atmospheric diffusion.
doi: 10.2172/5591108

Hanna, S., Brown, M., Camelli, F., Chan, S., Coirier, W., Hansen, O., ... Reynolds, R. (2006). Detailed simulations of atmospheric flow and dispersion in urban downtown areas by computational fluid dynamics (cfd) models - an application of five cfd models to manhattan. *Bulletin of the American Meteorological Society*, *87*, 1713-1726. doi: 10.1175/BAMS-87-12-1713

Idrissi, M. S., Lakhal, F. A., Salah, N. B., & Chrigui, M. (2018). Cfd modeling of air pollution dispersion in complex urban area. In M. Haddar, F. Chaari, A. Benamara, M. Chouchane, C. Karra, & N. Aifaoui (Eds.), *Design and modeling of mechanical systems—iii* (p. 1191-1203). Cham: Springer International Publishing.

Jackson, R. B., Saunois, M., Bousquet, P., Canadell, J. G., Poulter, B., Stavert, A. R., ... Tsuruta, A. (2020). Increasing anthropogenic methane emissions arise equally from agricultural and fossil fuel sources. *Environmental Research Letters*, *15*(7), 071002. Retrieved from `https://doi.org/10.1088%2F1748-9326%2Fab9ed2` doi: 10.1088/1748-9326/ab9ed2

Jeanjean, A., Hinchliffe, G., McMullan, W., Monks, P., & Leigh, R. (2015). A cfd study on the effectiveness of trees to disperse road traffic emissions at a city scale. *Atmospheric Environment*, *120*, 1 - 14. doi: https://doi.org/10.1016/j.atmosenv.2015.08.003

Kato, M., & Launder, B. (1993). The modelling of turbulent flow around stationary and vibrating square cylinders. *Proc. 9th Symposium on Turbulent Shear Flows*, 10.4.1-10.4.6.

Klote, J. H. (1991). A general routine for analysis of stack effect. *U.S. Department of Commerce*, 51.

Landeshauptstadt München. (2019). *Oktoberfest-bilanz 2019: Zahlen und fakten.* `https://www.oktoberfest.de/magazin/oktoberfest-news/2019/die-offizielle-oktoberfest-bilanz-2019`. (Online; accessed 21-January-2020)

Lateb, M., Meroney, R., Yataghene, M., Fellouah, H., Saleh, F., & Boufadel, M. (2016). On the use of numerical modelling for near-field pollutant dispersion in urban environments- a review. *Environmental Pollution*, *208*, 271 - 283. (Special Issue: Urban Health and Wellbeing) doi: https://doi.org/10.1016/j.envpol.2015.07.039

LI-COR Inc. (2018). Precisetechdesign-gas-analyzers-brochure-17927 [Computer software manual]. (LI-COR Trace Gas Analyzers)

Lide, D. (2004). *Crc handbook of chemistry and physics, 85th edition* (No. Bd. 85). Taylor & Francis.

Maronga, B., Banzhaf, S., Burmeister, C., Esch, T., Forkel, R., Frhlich, D., ... Raasch, S. (2020). Overview of the palm model system 6.0. *Geoscientific Model Development*, *13*, 1335-1372. doi: 10.5194/gmd-13-1335-2020

Meroney, R., Ohba, R., Leitl, B., Kondo, H., Grawe, D., & Tominaga, Y. (2016). Review of cfd guidelines for dispersion modeling. *Fluids*, *1*, 14. doi: 10.3390/fluids1020014

Mikaloff-Fletcher, S. E., & Schaefer, H. (2019). Rising methane: A new climate challenge. *Science*, *364*, 932-933.

Nakibolu, G., Gorl, C., Horvth, I., van Beeck, J., & Blocken, B. (2009). Stack gas dispersion measurements with large scale-piv, aspiration probes and light scattering techniques and comparison with cfd. *Atmospheric Environment*, *43*(21), 3396 - 3406. Retrieved from `http://www.sciencedirect.com/science/article/pii/S1352231009002817` doi: https://doi.org/10.1016/j.atmosenv.2009.03.047

Nisbet, E. G., Fisher, R. E., Lowry, D., France, J. L., Allen, G., Bakkaloglu, S., ... Zazzeri, G. (2020). Methane mitigation: Methods to reduce emissions, on the path to the paris agreement. *Reviews of Geophysics*, *58*(1), e2019RG000675. Retrieved from `https://agupubs.onlinelibrary.wiley.com/doi/abs/10.1029/2019RG000675` (e2019RG000675 2019RG000675) doi: https://doi.org/10.1029/2019RG000675

Nisbet, E. G., Manning, M. R., Dlugokencky, E. J., Fisher, R. E., Lowry, D., Michel, S. E., ... White, J. W. C. (2019). Very strong atmospheric methane growth in the 4 years 20142017: Implications for the paris agreement. *Global Biogeochemical Cycles*, *33*(3), 318-342. Retrieved from https://agupubs.onlinelibrary.wiley.com/doi/abs/10.1029/2018GB006009 doi: https://doi.org/10.1029/2018GB006009

NOAA National Centers for Environmental Information. (2020). *State of the climate: Global climate report for annual 2019.* https://www.ncdc.noaa.gov/sotc/global/201913. (Online; accessed 21-January-2020)

Nozu, T., & Tamura, T. (2012). Les of turbulent wind and gas dispersion in a city. *Journal of Wind Engineering and Industrial Aerodynamics*, *s 104106*, 492499. doi: 10.1016/j.jweia.2012.02.024

Pasquill, F. (1966). Lagrangian similarity and vertical diffusion from a source at ground level. *Quarterly Journal of the Royal Meteorological Society*, *92*(392), 185-195. Retrieved from https://rmets.onlinelibrary.wiley.com/doi/abs/10.1002/qj.49709239202 doi: https://doi.org/10.1002/qj.49709239202

Pasquill, F. (1969). The influence of the turning of wind with height on crosswind diffusion. *Philosophical Transactions of the Royal Society of London. Series A, Mathematical and Physical Sciences*, *265*(1161), 173–181. Retrieved from http://www.jstor.org/stable/73723

Pasquill, F. (1979). Atmospheric dispersion modeling. *Journal of the Air Pollution Control Association*, *29*(2), 117-119. Retrieved from https://doi.org/10.1080/00022470.1979.10470764 doi: 10.1080/00022470.1979.10470764

Patnaik, G., Boris, J., Young, T., & Grinstein, F. (2007). Large scale urban contaminant transport simulations with miles. *Journal of Fluids Engineering-transactions of The Asme - J FLUID ENG*, *129*. doi: 10.1115/1.2801368

Plant, G., Kort, E. A., Floerchinger, C., Gvakharia, A., Vimont, I., & Sweeney, C. (2019). Large fugitive methane emissions from urban centers along the u.s. east coast. *Geophysical Research Letters*, *46*(14), 8500-8507. Retrieved from https://agupubs.onlinelibrary.wiley.com/doi/abs/10.1029/2019GL082635 doi: https://doi.org/10.1029/2019GL082635

Pope, S. B. (2000). *Turbulent flows.* Cambridge University Press. doi: 10.1017/CBO9780511840531

Richards, P., & Hoxey, R. (1993). Appropriate boundary conditions for computational wind engineering models using the k-ϵ turbulence model. In S. Murakami (Ed.), *Computational wind engineering 1* (p. 145 - 153). Oxford: Elsevier. doi: https://doi.org/10.1016/B978-0-444-81688-7.50018-8

Riddle, A., Carruthers, D., Sharpe, A., McHugh, C., & Stocker, J. (2004). Comparisons between fluent and adms for atmospheric dispersion modelling. *Atmospheric Environment*, *38*(7), 1029 - 1038. Retrieved from http://www.sciencedirect.com/science/article/pii/S1352231003009713 doi: https://doi.org/10.1016/j.atmosenv.2003.10.052

Sadeghzadeh, M. (2007). Utilization of domestic gas heater exhaust energy for heating water. *International Energy Journal*, *8*, 63-70.

Saunois, M., Stavert, A. R., Poulter, B., Bousquet, P., Canadell, J. G., Jackson, R. B., ... Zhuang, Q. (2020). The global methane budget 2000–2017. *Earth System Science Data*, *12*(3), 1561–1623. Retrieved from https://essd.copernicus.org/articles/12/1561/2020/ doi: 10.5194/essd-12-1561-2020

Shi, R., Cui, G., Wang, Z., Xu, C., & Zhang, Z. (2008). Large eddy simulation of wind field and plume dispersion in building array. *Atmospheric Environment*, *42*(6), 1083 - 1097. doi: https://doi.org/10.1016/j.atmosenv.2007.10.071

Sonderfeld, H., Bösch, H., Jeanjean, A. P. R., Riddick, S. N., Allen, G., Ars, S., ... Pitt, J. (2017). Ch4 emission estimates from an active landfill site inferred from a combined approach of cfd modelling and in situ ftir measurements. *Atmospheric Measurement Techniques*, *10*(10), 3931–3946. Retrieved from https://www.atmos-meas-tech.net/10/3931/2017/ doi: 10.5194/amt-10-3931-2017

Toja-Silva, F., Chen, J., Hachinger, S., & Hase, F. (2017). Cfd simulation of co2 dispersion from urban thermal power plant: Analysis of turbulent schmidt number and comparison with gaussian plume model and measurements. *Journal of Wind Engineering and Industrial Aerodynamics*, *169*, 177-193. doi: 10.1016/j.jweia.2017.07.015

Toja-Silva, F., Peralta, C., Lopez-Garcia, O., Navarro, J., & Cruz, I. (2015). Roof region dependent wind potential assessment with different rans turbulence models. *Journal of Wind Engineering and Industrial Aerodynamics*, *142*, 258 - 271. doi: https://doi.org/10.1016/j.jweia.2015.04.012

Tominaga, Y., & Stathopoulos, T. (2007). Turbulent schmidt numbers for cfd analysis with various types of flowfield..

Tominaga, Y., & Stathopoulos, T. (2013). Cfd simulation of near-field pollutant dispersion in the urban environment: A review of current modeling techniques. *Atmospheric Environment*, *79*, 716 - 730. doi: https://doi.org/10.1016/j.atmosenv.2013.07.028

Tominaga, Y., & Stathopoulos, T. (2016). Ten questions concerning modeling of near-field pollutant dispersion in the built environment. *Building and Environment*, *105*, 390 - 402. doi: https://doi.org/10.1016/j.buildenv.2016.06.027

Tran, V., Ng, E., & Skote, M. (2019). Cfd simulation of dense gas dispersion in neutral atmospheric boundary layer with openfoam. *Meteorology and Atmospheric Physics*, *132*, 273-285.

Tsuchiya, M., Murakami, S., Mochida, A., Kondo, K., & Ishida, Y. (1997). Development of a new k-ϵ model for flow and pressure fields around bluff body. *Journal of Wind Engineering and Industrial Aerodynamics*, *67-68*, 169 - 182. (Computational Wind Engineering) doi: https://doi.org/10.1016/S0167-6105(97)00071-8

Van Hooff, T., & Blocken, B. (2010). On the effect of wind direction and urban surroundings on natural ventilation of a large semi-enclosed stadium. *Computers and Fluids*, *39*(7), 1146 - 1155. doi: https://doi.org/10.1016/j.compfluid.2010.02.004

Varon, D. J., McKeever, J., Jervis, D., Maasakkers, J. D., Pandey, S., Houweling, S., ... Jacob, D. J. (2019). Satellite discovery of anomalously large methane point sources from oil/gas production. *Geophysical Research Letters*, *46*(22), 13507-13516. Retrieved from `https://agupubs.onlinelibrary.wiley.com/doi/abs/10.1029/2019GL083798` doi: https://doi.org/10.1029/2019GL083798

Wang, Y., Huang, H., & Lida, H. (2015). Numerical study of leaked natural gas dispersion within an urban street canyon considering the distribution of ground surface flux. In *The 4th international conference on civil engineering and urban planning (ceup2015)* (Vol. 61-64).

Wingstedt, E. M. M., Vartdal, M., & Pettersson Reif, B. A. (2017). Large-eddy simulations of dense-gas dispersion within a high-reynolds number turbulent boundary layer. *Physics of Fluids*, *29*(9), 095103. doi: 10.1063/1.4999466

Yap, C. (1987). *Turbulent heat and momentum transfer in recirculating and impinging flows* (Unpublished doctoral dissertation). Faculty of Technology, University of Manchester, United Kingdom.

Yu, H., & Thé, J. (2017). Simulation of gaseous pollutant dispersion around an isolated building using the k sst (shear stress transport) turbulence model. *Journal of the Air & Waste Management Association*, *67*(5), 517-536. Retrieved from `https://doi.org/10.1080/10962247.2016.1232667` (PMID: 27650217) doi: 10.1080/10962247.2016.1232667

Zeebe, R. E., Ridgwell, A., & Zachos, J. C. (2016). Anthropogenic carbon release rate unprecedented during the past 66 million years. *Nature Geoscience*, *9*, 325-329.

Zhao, X., Marshall, J., Hachinger, S., Gerbig, C., Frey, M., Hase, F., & Chen, J. (2019). Analysis of total column co2 and ch4 measurements in berlin with wrf-ghg. *Atmospheric Chemistry and Physics*, *19*(17), 11279–11302. Retrieved from https://acp.copernicus.org/articles/19/11279/2019/ doi: 10.5194/acp-19-11279-2019